

## Compression plasma flows interaction with nickel based binary, ternary and high-entropy alloys

N.N. Cherenda<sup>1,\*</sup>, S.S. Huang<sup>2</sup>, K.V. Bernat<sup>1</sup>, V.M. Astashynski<sup>3</sup>, A.M. Kuzmitski<sup>3</sup>, A.V. Basalai<sup>4</sup>

<sup>1</sup>Belarussian State University, Minsk, Belarus

<sup>2</sup>Key Laboratory of Materials Modification by Laser, Ion and Electron Beams (Dalian University of Technology), Ministry of Education, Dalian, China

<sup>3</sup>A.V.Lyikov Heat and Mass Transfer Institute of the National Academy of Sciences of Belarus, Minsk, Belarus

<sup>4</sup>State Scientific Institution "The Physical Technical Institute of the National Academy of sciences of Belarus, Minsk, Belarus

\*cherenda@bsu.by

**Abstract.** Microstructure, phase and element composition of nickel-based alloys  $\text{Ni}_{0.6}\text{Co}_{0.2}\text{X}_{0.2}$  (where X = Fe, Co, V) and CoCrFeNiMn alloy after compression plasma impact were investigated in this work. X-ray, scanning electron microscopy, energy-dispersion X-ray microanalysis and microhardness measurements were used as investigation techniques. Formation or enhancement of (100) texture after plasma treatment was found for binary and triple Ni based alloys. Plasma impact with  $\text{Ni}_{0.6}\text{Co}_{0.2}\text{V}_{0.2}$  alloy led to vanadium surface segregation and formation of  $\text{V}_2\text{O}_3$  oxide. Variation of the alloys element composition resulted in the change of surface erosion intensity during plasma treatment due to the influence on the viscosity and surface tension of the melt.  $\text{Ni}_{0.6}\text{Co}_{0.2}\text{Fe}_{0.2}$  and NiCoFeCrMn alloys possessed highest erosion intensity.

**Keywords:** high-entropy alloys, nickel alloys, compression plasma flows, microstructure, phase transformations.

### 1. Introduction

High-entropy alloys with unique properties have attracted considerable attention of researchers around the world [1]. Due to the unique physicochemical properties (corrosion resistance, high thermal stability, wear resistance, increased strength and ductility, etc.), the application of this type of alloy can be very wide [2]. Cantor alloy is one of the most famous high-entropy alloys, which has excellent ductility and fracture toughness [3, 4]. Previous studies have shown that resistance of CoCrFeNiMn alloy under He ions irradiation was higher than that of SS304 steel [5]. High migration barrier of radiation point defects due to the local lattice distortions can be the cause of this effect [5]. High radiation stability allows the application of these alloys in the nuclear industry.

Another key issue of materials application in nuclear and thermonuclear energetics is the resistance of the material to high thermal loads. Quasi-stationary plasma accelerators are widely used to test the resistance of first wall materials of the thermonuclear reactors to plasma disruption events. [6, 7]. Studying the stability of the structure and mechanical properties of Cantor alloy when exposed to high-temperature plasma flows was the aim of this work. Besides that a few binary and triple Ni based alloys were investigated just to determine the influence of Cantor alloy components on the effects observed during plasma impact.

### 2. Experimental

Binary and ternary nickel-based alloys  $\text{Ni}_{0.6}\text{Co}_{0.2}\text{X}_{0.2}$  (where X = Fe, Co, V) that contained components of Cantor alloy as well as CoCrFeNiMn alloy were investigation objects. Alloys were prepared in a vacuum induction furnace. Details of samples preparation can be found in [8]. Compression plasma flows (CPF) were obtained in nitrogen atmosphere using a gas-discharge magneto-plasma compressor of compact geometry [9]. Duration of the plasma pulse was about 100  $\mu\text{s}$ . Treatment was carried out with three pulses at the energy density absorbed by the surface  $\sim 12 \text{ J/cm}^2$  per pulse. The phase composition of the surface layer was investigated by means of the X-ray diffraction method (XRD) using the Ultima IV RIGAKU diffractometer in Bragg-Brentano geometry with parallel beams in Cu  $K\alpha$  radiation. The surface morphology of the samples was

studied using scanning electron microscopy (SEM) on a LEO1455VP microscope combined with an Oxford X-ray detector for energy-dispersion X-ray microanalysis. The samples weight was determined before and after CPF treatment by analytical balance RADWAG AS 60/220/C/2/N with the accuracy of  $\pm 0.05$  mg. Vickers microhardness measurement was also carried out to characterize mechanical properties of the surface layer.

### 3. Results

Treatment of metals by CPF in the used energy density range absorbed by the surface led to the melting of the surface layer, appearance of convection processes in the melt and following crystallization in conditions of high-cooling speed (up to  $10^7$  K/s). CPF impact with the surface of nickel based alloys resulted in the change of their microstructure and phase composition. Fig. 1 and Fig. 2 show the XRD patterns of alloys before and after CPF impact. In initial state the structure of all alloys was a solid solution based on an fcc crystalline lattice. Analysis of the structural-phase state showed that the intensity of the (200) diffraction line increased in all binary and triple alloys after plasma treatment. This is especially noticeable in the  $\text{Ni}_{0.6}\text{Co}_{0.2}\text{Fe}_{0.2}$  sample (Fig. 1).

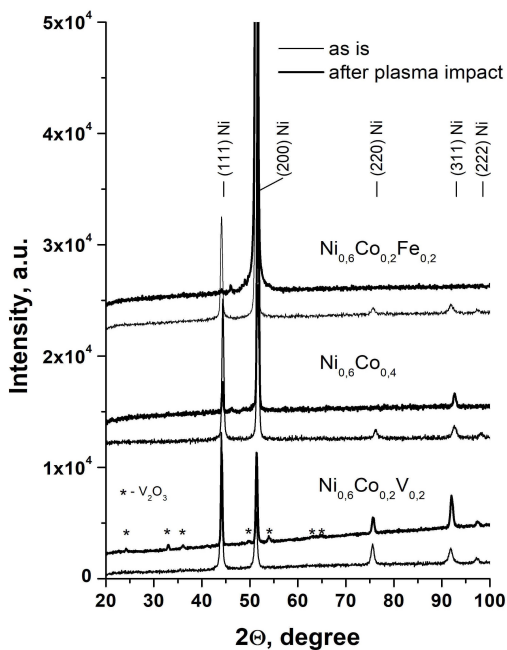


Fig. 1. XRD diffraction patterns of binary and ternary Ni based alloys before and after CPF treatment.

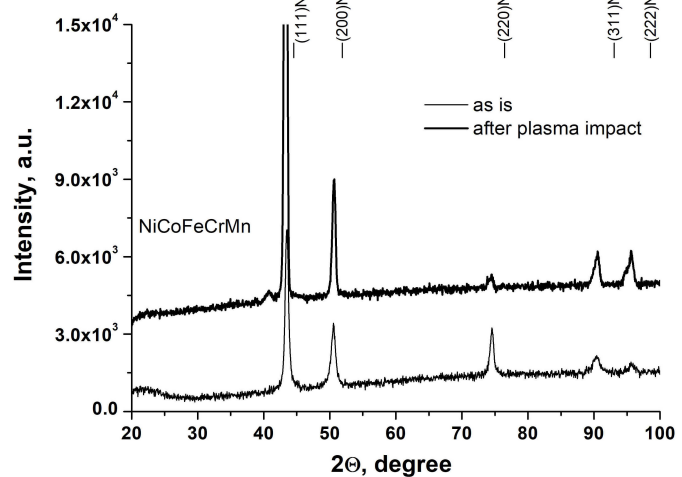


Fig. 2. XRD diffraction patterns of  $\text{NiCoFeCrMn}$  alloy before and after CPF treatment.

This behavior may be due to the following effect. It is known that under conditions of high thermal and concentration supercooling, for example, under laser irradiation, the formation of a cellular-dendritic structure during crystallization from the melt is possible. In metals with an fcc crystal structure, dendrite growth typically occurs in the  $\langle 100 \rangle$  direction, which coincides with the direction of heat removal. This is caused by the thermodynamic condition under which the surface elements of crystallites protruding in the melt should have a maximum growth rate. This condition is realized in fcc metals if the dendrite axis coincides with the direction of the edge of the cube, which is the axis of the pyramid formed by four densely packed  $\{111\}$  planes, that is, with a  $\langle 100 \rangle$  type direction [10].

In addition, new diffraction peaks appeared in the  $\text{Ni}_{0.6}\text{Co}_{0.2}\text{V}_{0.2}$  sample that can be attributed to the formation of  $\text{V}_2\text{O}_3$  oxide. This effect was observed due to interaction of residual atmosphere

atoms (molecules) with the atoms of heated surface [11]. Formation of surface films should occur due to diffusion of atoms from the bulk to the surface. The data of energy-dispersion microanalysis showed that concentration of vanadium in the analyzed layer was increased up to 39 at.% while its concentration in initial alloy was 20 at.%. Concentration of elements in the surface layer of other alloys was not changed after plasma impact.

Analysis of XRD patterns of Cantor alloy before and after plasma impact (Fig. 2) showed that (311) and (222) diffraction patterns were split after impact and have a “shoulder” on the left slope of diffraction lines. Thus one could conclude that CPF treatment led to the formation of a new phase with fcc crystalline structure and lattice parameter larger than that of initial alloy (0.3600 nm).

Surface morphology of alloys after plasma treatment is shown in Fig. 3. One can see that surface roughness is strongly dependent on the alloy composition. Ni alloy with vanadium possessed more developed surface roughness in contrast to the alloy containing iron and Cantor alloy. Besides that a strong redistribution of elements at the surface was observed for  $\text{Ni}_{0.6}\text{Co}_{0.2}\text{V}_{0.2}$  alloy (Fig. 3a). Brighter areas (due to the element contrast in back scattered electrons) were enriched with Co and Ni atoms.

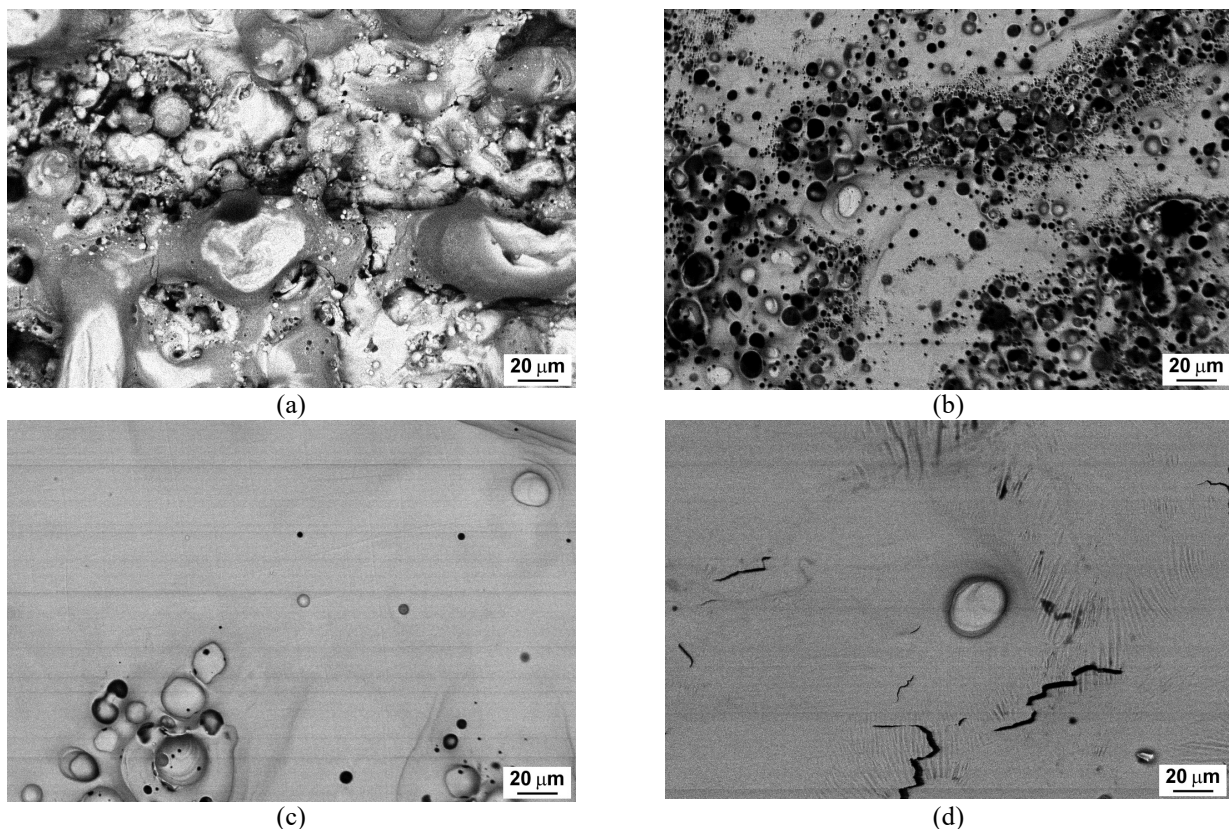


Fig. 3. SEM surface morphology of alloys after plasma impact:  $\text{Ni}_{0.6}\text{Co}_{0.2}\text{V}_{0.2}$  (a),  $\text{Ni}_{0.6}\text{Co}_{0.4}$  (b),  $\text{Ni}_{0.6}\text{Co}_{0.2}\text{Fe}_{0.2}$  (c), NiCoFeCrMn (d).

CPF impact with Ni based alloys led to its surface erosion (Fig 4). The highest value of the removed mass ( $2.22 \text{ mg/cm}^2$ ) was observed for the Cantor alloy, the lowest ( $1.67 \text{ mg/cm}^2$ ) for the  $\text{Ni}_{0.6}\text{Co}_{0.2}\text{V}_{0.2}$  alloy. The hydrodynamic flow of the melt during plasma impact was the main reason of this effect. The study of this process, which occurs under the action of high-temperature plasma flows on materials, is most relevant for studying the processes of plasma disruption and transient processes in TOKAMAK type thermonuclear reactors. In particular, it was shown in [12] that under the action of plasma flows generated by a quasi-steady-state plasma accelerator, a crater is formed

on the tungsten surface, onto the edges of which the plasma spreading along the surface squeezes the melt. A similar result was obtained on steel after exposure to compression plasma flows [13]. An increase in both the absorbed energy density and the number of pulses should lead to the growth of the erosion intensity [13].

Thus, variation of the alloys element composition resulted in the change in surface erosion intensity due to element composition influence on the viscosity and surface tension of the melt. In particular,  $\text{Ni}_{0.6}\text{Co}_{0.2}\text{Fe}_{0.2}$  and  $\text{NiCoFeCrMn}$  alloys with relatively smooth surface after plasma impact (Fig. 3) possessed highest erosion intensity that can be possibly connected with low melt viscosity. The lowest value of deleted mass for the  $\text{Ni}_{0.6}\text{Co}_{0.2}\text{V}_{0.2}$  alloy can also be explained by formation of  $\text{V}_2\text{O}_3$  surface oxide film with high crystallization temperature — 1967 °C, that hinder hydrodynamic movement of the melt [14].

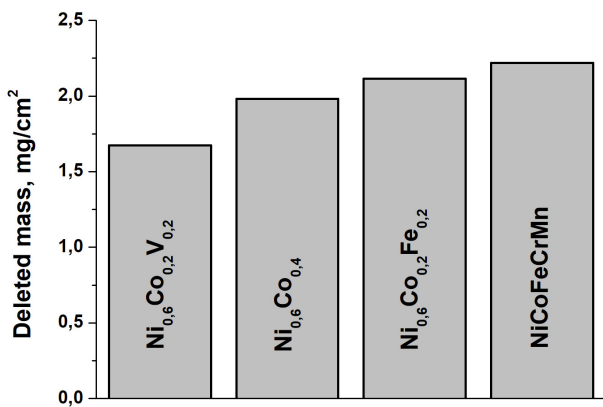


Fig. 4. Mass deleted from the surface of Ni based alloys during CPF treatment.

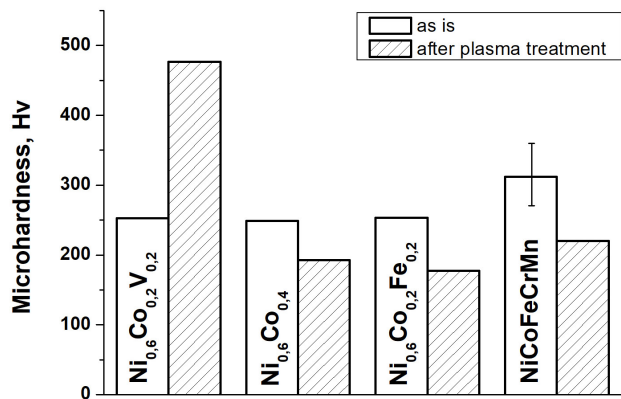


Fig. 5. Microhardness of Ni based alloys before and after CPF treatment.

Formation of  $\text{V}_2\text{O}_3$  oxide could also lead to microhardness increase after CPF impact from 253 to 477 Hv (Fig. 5). Microhardness decrease was observed for other types of alloys. Such behavior can be explained by preliminary cold working of alloys surface during grinding and following annealing after CPF treatment.

#### 4. Conclusion

Treatment of Ni based alloys by three pulses of compression plasma flows at the density of the energy absorbed by the surface layer 12 J/cm<sup>2</sup> per pulse led to the melting of the surface layer. Formation or enhancement of (100) texture in the crystallized layer of  $\text{Ni}_{0.6}\text{Co}_{0.2}\text{X}_{0.2}$  (where X = Fe, Co, V) alloys was found. Interaction of residual atmosphere atoms (molecules) with the atoms of  $\text{Ni}_{0.6}\text{Co}_{0.2}\text{V}_{0.2}$  heated surface resulted in the increase of vanadium concentration in the analyzed layer up to 39 at.% and formation of  $\text{V}_2\text{O}_3$  oxide. Concentration of elements in the surface layer of other alloys was not changed after plasma impact. The findings showed that surface morphology was strongly dependent on the alloy composition. Ni alloy with vanadium possessed more developed surface roughness in contrast to the alloy containing Fe atoms and Cantor alloy.

CPF impact with Ni based alloys led to its surface erosion. The highest value of the removed mass (2.22 mg/cm<sup>2</sup>) was observed for the Cantor alloy, the lowest (1.67 mg/cm<sup>2</sup>) for the  $\text{Ni}_{0.6}\text{Co}_{0.2}\text{V}_{0.2}$  alloy. The lowest value of deleted mass for the  $\text{Ni}_{0.6}\text{Co}_{0.2}\text{V}_{0.2}$  alloy could be explained by formation of  $\text{V}_2\text{O}_3$  surface oxide film that hinder hydrodynamic movement of the melt.

Formation of  $\text{V}_2\text{O}_3$  oxide could also lead to microhardness increase after CPF impact from 253 to 477 Hv. Microhardness decrease was observed for other types of alloys.

## 5. References

- [1] Y.F. Ye, Q. Wang, J. Lu, C.T. Liu and Y. Yang, High-entropy alloy: challenges and prospects, *Materials Today*, vol. **19**, 349–362, 2016, doi: 10.1016/j.mattod.2015.11.026
- [2] D.B. Miracle, O.N. Senkov, A critical review of high entropy alloys and related concepts, *Acta Materialia*, vol. **122**, 448–511, 2017, doi: 10.1016/j.actamat.2016.08.081
- [3] B. Cantor, Multicomponent high-entropy Cantor alloys, *Progress in Materials Science*, vol. **120**, 100754, 2020, doi: 10.1016/j.pmatsci.2020.100754
- [4] Z. Zeng, M. Xiang, D. Zhang, J. Shi, W. Wang, X. Tang, W. Tang, Y. Wang, X. Ma, Z. Chen, W. Ma, K. Morita, Mechanical properties of Cantor alloys driven by additional elements: a review, *Journal of Materials Research and Technology*, vol. **15**, 1920, 2021, doi: 10.1016/j.jmrt.2021.09.019
- [5] S.S. Huang, H.Q. Guan, Z.H. Zhong, M. Miyamoto, Q. Xu, Effect of He on the irradiation resistance of equiatomic CoCrFeMnNi high-entropy alloy, *Journal of Nuclear Materials*, vol. **561**, 153525, 2022, doi: 10.1016/j.jnucmat.2022.153525
- [6] I.E. Garkusha, V.A. Makhraj, V.V. Chebotarev, I. Landman, V.I. Tereshin, N.N. Aksenov, A.N. Bandura, Experimental study of plasma energy transfer and material erosion under ELM-like heat loads, *Journal of Nuclear Materials*, vol. **390–391**, 814, 2009, doi: 10.1016/j.jnucmat.2009.01.215
- [7] S. Borthakur, N. Talukdar, N.K. Neog, T.K. Borthakur, Design of a coaxial plasma accelerator for fusion relevant material studies, *Fusion Engineering and Design*, vol. **122**, 131, 2017, doi: 10.1016/j.fusengdes.2017.09.001
- [8] Q. Xu, H.Q. Guan, Z.H. Zhong, S.S. Huang, J.J. Zhao, Irradiation resistance mechanism of the CoCrFeMnNi equiatomic high-entropy alloy, *Scientific Reports*, vol. **11**, 608, 2021, doi: 10.1038/s41598-020-79775-0
- [9] N.N. Cherenda, A.V. Basalai, V.I. Shymanski, V.V. Uglov, V.M. Astashynski, A.M. Kuzmitski, A.P. Laskovnev, G.E. Remnev, Modification of Ti-6Al-4V alloy element and phase composition by compression plasma flows impact, *Surface & Coatings Technology*, vol. **355C**, 148, 2018, doi: 10.1016/j.surfcoat.2018.02.048
- [10] N.N. Cherenda, A.V. Basalai, V.V. Uglov, A.P. Laskovnev, V.M. Astashynski, A.M. Kuzmitski, Phase composition and mechanical properties of Cu-Ti alloys synthesized in the surface layer of copper by plasma impact on the Ti/Cu system, *Vacuum*, vol. **167**, 452, 2019, doi: 10.1016/j.vacuum.2019.06.033
- [11] N.N. Cherenda, V.V. Uglov, A.K. Kuleshov, V.M. Astashynski, A.M. Kuzmitski, Surface nitriding and alloying of steels with Ti and Nb atoms by compression plasma flows treatment, *Vacuum*, vol. **129**, 170, 2016, doi: 10.1016/j.vacuum.2016.03.019
- [12] V.I. Tereshin, I.E. Garkusha, A.N. Bandura, O.V. Byrka, V.V. Chebotarev, V.A. Makhraj, D.G. Solyakov, H. Wuerz, Influence of plasma pressure gradient on melt layer macroscopic erosion of metal targets in disruption simulation experiments, *Journal of Nuclear Materials*, vol. **313–316**, 685, 2003, doi: 10.1016/S0022-3115(02)01361-2
- [13] A.Ya. Leyvi, N.N. Cherenda, V.V. Uglov, A.P. Yalovets, The impact of a shock-compressed layer on the mass transfer of target material during processing compression plasma flows, *Resource-Efficient Technologies*, vol. **3**, 222, 2017, doi: 10.1016/j.reffit.2017.06.003
- [14] P. Shvets, O. Dikaya, K. Maksimova, A. Goikhman, A review of Raman spectroscopy of vanadium oxides, *J Raman Spectrosc.*, vol. **50**, 1226, 2019, doi: 10.1002/jrs.5616